RSC Advances

ROYAL SOCIETY OF CHEMISTRY

www.rsc.org/advances

RSC Advances

RSCPublishing

PAPER

Microwave Assisted Synthesis of Mesoporous $NiCo_2O_4$ Nanosheets as Electrode Material for Advanced Flexible Supercapacitors

Cite this: DOI: 10.1039/b000000x

Received ooth February 2015,
Accepted ooth February 2015

DOI: 10.1039/ b000000x

www.rsc.org/advances

Syed Khalid,[a] Chuanbao Cao,*[a] Aziz Ahmad,[b] Lin Wang,[a] Muhammad Tanveer,[a] Imran Aslam,[a] Muhammad Tahir,[a] Faryal Idrees,[a] and Youqi Zhu[a]

Mesoporous nickel cobaltite ($NiCo_2O_4$) nanosheets are synthesized using cost effective, ultra fast and environmental friendly microwave assisted heating method followed by a post-calcining process of as-prepared precursors. XRD, XPS, BET, SEM, TEM and HRTEM methods are used to characterize nanosheets. The as-prepared nanosheets with thickness of around 2 nm possess many interparticle mesopores. The nanosheets have mesoporous structure, high specific surface area (111.15 $m^2\ g^{-1}$), large pore volume (0.3033 $cm^3\ g^{-1}$) and narrow pore size distribution (2.25-10 nm). The flexible supercapacitor working electrode of mesoporous $NiCo_2O_4$ nanosheets is prepared on carbon cloth. Cyclic voltammetry, chronopotentiometry and impedance spectroscopy measurements are used to investigate electrochemical performance of as-prepared mesoporous $NiCo_2O_4$ nanosheets/carbon cloth electrode. The mesoporous $NiCo_2O_4$ nanosheets exhibit specific capacitance of 292.5 and 200 F g^{-1} in 2M KOH aqueous electrolyte at current densities of 1 and 8 A g^{-1} respectively. The cyclic performance indicates excellent capacitance retention of 94.5 % after 2000 cycles at current density of 3 A g^{-1}. The excellent cyclic stability can be attributed to the mesoporous, high specific surface area, large pore volume and narrow pore distribution of nanosheets. The synthesis of mesoporous $NiCo_2O_4$ nanosheets using microwave method proves to be excellent electrode material for advanced flexible supercapacitor.

Introduction

In recent years, the research focused on developing smart, low cost, environmentally friendly and flexible energy devices for portable electronics applications and electric vehicles.[1-3] Among various energy storage devices, supercapacitors have been considered as the strong candidate owing to their advantages of higher power density, faster charge/discharge process and longer lifespan, which makes them attractive as power resources in high power portable electronic devices and electric vehicles.[4-9] In the perspective of flexible devices, ITO glass and other metal current collectors are not suitable due to their non-flexibility and lower mechanical strength. Secondly it is also important to avoid the use of Ni foam as current collector because it can contribute substantial errors towards the specific capacitance values of the test electrode materials during electrochemical performance investigation.[10,11] The carbon cloth is one of the best alternative because of its flexibility, light weight, good electrical conductor, high porosity and chemical compatibility.[12]

Based on the charge storage mechanism electrochemical capacitors (ECs) have been categorized as electrochemical double layer capacitors (EDLCs) and pseudocapacitors.[13] EDLCs store energy based on adsorption of charges at the electrode/electrolyte interfaces whereas pseudocapacitors store energy based on fast reversible redox reactions at the surface of active material.[13] Unfortunately, the low specific capacitance (SC) of EDLCs cannot meet the ever-growing need for peak-power assistance in electronic devices, and so on. Thus, growing interest in using pseudocapacitive materials for ECs has been triggered because the energy density associated with Faradaic reactions is substantially larger by at least one order of magnitude than that of EDLCs.[14-16] The most notable pseudocapacitive materials studied is RuO_2, however, its large-scale application is hindered by the very high cost and rareness of the Ru element.[17,18] Therefore, low cost transition metal oxides have been developed as electrode materials for electrochemical capacitors, primarily including binary compounds of MnO_2,[19,20] NiO,[21,22] CoO,[23] Co_3O_4,[24,25] and $Ni(OH)_2$ [26-28] etc.

In particular spinel nickel cobaltite $NiCo_2O_4$ supercapacitor has been conceived as a promising cost effective and scalable alternative since

[a] Research Center of Materials Science, Beijing Institute of Technology, Beijing 100081, P. R. China. E-mail: cbcao@bit.edu.cn; Fax: +86 10 6891 2001; Tel: +86 10 6891 3792

[b] National Center for Nanoscience and Technology, Chinese Academy of Sciences, Beijing 100190, P. R. China

† Electronic supplementary information (ESI) available: X-ray diffraction pattern of as-synthesized precursor, CV scan of carbon cloth, oxidation current of hybrid electrode as a function of square root of scan rate, CV scan of hybrid electrode at higher scan rate (50 and 60 mV s^{-1}), Coulombic efficiency of electrode at 3 A g^{-1}, charge - discharge curves of first ten, intermediate five and last five cycles at current densities 1 and 3 A g^{-1}, cycle performance at current density 8 A g^{-1}, cycle performance at current density 3 A g^{-1} in the bend state, SEM images of electrode before and after cycle test, simulated impedence values of fresh and used electrodes. See DOI: 10.1039/b000000x

it offers many advantages such as low cost, abundant resources and environmental friendliness.[13,29-31] The spinel $NiCo_2O_4$ possesses much better electrical conductivity, at least two orders of magnitude higher, and better electrochemical activity than nickel oxides or cobalt oxides.[32] The higher electrical conductivity is due to electron transfer taking place at relatively low activation energy between cations.[13] The higher electrochemical performance can be attributed to its offering richer redox reactions, including contributions from both nickel and cobalt ions, than those of the monometallic nickel oxides and cobalt oxide.[11-14] The electrode material properties and morphology are the key factor for the high Performance supercapacitor.[5] The electrode material should have high specific surface area, ordered pore size distribution, high conductivity, long term cycle stability and electrochemical reproducibility.[5]

In order to develop the flexible supercapacitor, carbon cloth is one of the best choice because of its highly flexible nature, low cost, high electrical conductivity, higher mechanical strength and good corrosion resistance. Recently few papers have been published in which carbon cloth was used as the current collector.[33-36] N. Padmanathan et al. have grown $NiCo_2O_4$ nanowalls and nanoflakes on carbon cloth by a hydrothermal method.[33] D. Zhang et al have grown $NiCo_2O_4$ nanoneedle on carbon cloth by a hydrothermal method.[34] F. Luan et al. have grown NiO nanoflakes on carbon fiber cloth by a hydrothermal method for asymmetric supercapacitors.[35] H. Wang et al. have grown $NiCo_2O_4$ nanowires and nanosheets on carbon cloth by a hydrothermal method.[36] They reported specific capacitance of 245 F g^{-1} at 1 A g^{-1} with surface area (79.34 m^2 g^{-1}), pore volume (0.26 cm^3 g^{-1}) & pore distribution at (~ 4.86 nm) for $NiCo_2O_4$ nanowires and 123 F g^{-1} at 1 A g^{-1} with surface area (28.22 m^2 g^{-1}), pore volume (0.11 cm^3 g^{-1}) & pore distribution at (~ 3.04, 4.97, 12.46, and 26.44 nm) for $NiCo_2O_4$ nanosheets.[36] The nanosheets exhibited low specific capacitance due to their smaller specific surface area, smaller pore volume and disordered distribution of pores than that of nanowires.

To enhance the electrochemical performance of nanosheets, so it is imperative to synthesize nanosheets possessing high specific surface area, mesoporous porosity with ordered pore distribution and large pore volume. The high specific surface area will provide large amount of electroactive sites and the mesoporous porosity with ordered distribution of pores will facilitate the high transport rates for both electrons and electrolyte ions that simultaneously take part during Faradic reaction. The large pore volume can serve as the ion buffering reservoir which may accelerate the kinetic process of ion diffusion in electrode by minimizing the diffusion distance to the interior surfaces.

The microwave assisted heating method is simple and useful technique. This technique is considered as environmental friendly due to direct interaction of microwave with the reaction system instead of indirect heat transfer in the conventional heating method. It has been widely used for the synthesis of porous inorganic materials.[27,37,38] It's easy operation, short synthesis time, rapid and uniform volumetric heating are its great advantages.[39,40] It has already been widely used for preparation of number of both binary and ternary oxides.[41,42]

Herein, we report a microwave assisted synthetic strategy with simple thermal treatment to synthesize mesoporous $NiCo_2O_4$ nanosheets. The physical structure and electrochemical performance of as-synthesized material were characterized and investigated. The working electrode on carbon cloth was prepared by traditional slurry coating technique for electrochemical measurement. The as prepared $NiCo_2O_4$ nanosheets with thickness of around 2 nm possess mesoporous porosity within the nanosheets. In our case the as prepared material possess high specific surface area (111.15 m^2 g^{-1}), large pore volume (0.3033 cm^3 g^{-1}) and more ordered pore distribution at ~ 2.25 nm than that of reported nanosheets and nanowires.[36] The high surface area, ordered pore distribution and large pore volume of as-synthesized mesoporous nanosheets will endow high specific capacitance and excellent stability as an electrode material of flexible supercapacitor. The obtained mesoporous $NiCo_2O_4$ nanosheets on carbon cloth exhibit high specific capacitance of 292.5 F g^{-1} than that of reported for nanosheets 123 F g^{-1} and nanowires 245 F g^{-1} at 1 A g^{-1}.[36] The enhanced specific capacitance in comparison to the reported nanosheets and nanowires can be attributed due to mesoporous structure, high specific surface area, ordered pore distribution and large pore volume of electrode material. The mesoporous $NiCo_2O_4$ nanosheets exhibit excellent cyclic stability (94.5 and 90% capacitance retention after 2000 cycles at 3 and 8 A g^{-1} respectively) in 2 M KOH solution and thus a promising material for flexible advanced supercapacitors.

Experimental

All chemicals were of analytical grade and were used without further purification. The typical synthetic procedure is as follows: 4 mmole $Co(NO_3)_6 \cdot 6H_2O$, 2 mmole Ni $(NO_3)_6 \cdot 6H_2O$ and 24 mmole hexamethylene tetramine ($C_6H_{12}N_4$) were dissolved in 100 ml de-ionized water at room temperature followed by the magnetic stirring for 30 minutes. After stirring, the mixture was transferred to a 300 ml 3 necked flask. The three necked flask was placed in the chamber of microwave synthesis work station (MAS II, SINEO), the top of which was equipped with the water condenser. The solution was heated in a microwave oven under a medium high mode power 400 W at 100°C for 15 minutes. After cooling to room temperature naturally and standing for 10 hours, the precipitates were collected and centrifuged at 12,000 rpm for 4 min several times using de-ionized water and absolute ethanol and precipitates were then dried at 100°C in air overnight. Secondly, the precipitates was calcinated at 300°C in the atmospheric environment for 210 minutes. After the calcination process, the precursor was converted into black $NiCo_2O_4$ powder.

Characterization

Powder X-ray diffraction data were collected using a Philips X'Pert Pro MPD X-ray diffractometer with a Ni-filtered Cu Kα radiation (λ = 1.54178 Å) source with 2θ range from 10° to 80° at a scanning speed of 0.02°s^{-1} and tube voltage and current were set at 40 kV and 40 mA, respectively. The scanning electron microscopy (SEM) images were taken by a Hitachi S4800 field-emission scanning electron microscope to study the morphology of the samples. X-ray photoelectron spectrum (XPS) was measured by using an Thermo Scientific ESCALAB-250Xi spectrometer with a Al K_α (1,486.6 eV) as the X-ray source for excitation. Transmission electron microscopy (TEM) and high resolution TEM (HRTEM) images were captured on a JEOL JEM-2100 microscope to investigate the structure and morphology of the samples. In order to determine the thickness of nanosheets from the HRTEM, the electron beam was focussed on the vertical cross section at the top of one selected sheet. The nitrogen adsorption−desorption isotherms at 77 K were measured with a Micromeritics ASAP 2020 M analyzer and the specific surface area was determined by the Brunauer-Emmett-Teller (BET) method.

Fabrication and testing of working electrode

Carbon cloth (4 cm ×1 cm) was carefully cleaned in an ultrasound bath with Acetone, 1M HCl solution, deionized water and ethanol

for 15 minutes each, drying at 100°C for 24 hrs. The working electrode was prepared by mixing 80 wt % active material (as-prepared mesoporous $NiCo_2O_4$ nanosheets), 10 wt % conductivity agent (acetylene black) and 10 wt % polytetrafluoroethylene (PTFE) using mortal pestle. The small amount of ethanol was mixed in the prepared powder to make its slurry and then pasted it on cleaned carbon cloth (1 cm × 1 cm) using microinjector. The electrodes were dried at 80 °C for 24 hrs under vacuum to remove the moisture and solvent contents. The mass loading of active material on carbon cloth was around 1 mg cm^{-2}. Hg/HgCl(Saturated KCl solution) electrode and platinum wires were used as the reference and counter electrodes respectively. The electrochemical behavior of the working electrode was analyzed in 2 M KOH electrolytes in a three-electrode cell. The electrochemical performances of working electrode were examined using a cyclic voltammetry (CV) , electrochemical impedance spectra (EIS) measurements by IM6e electrochemical workstation and a galvanostatic charging-discharging or chronopotentiomerty (CP) test via LAND CT2001 tester. All tests were carried out at room temperature. CV tests were usually cycled between the voltage of -0.1V and 0.4 V with scan rates ranged from 2 to 60 mV s^{-1}, CP measurements were generally cycled between the voltage of -0.05 V and 0.35 V with current densities varied from 1 to 8 A g^{-1}, EIS experiments were taken under a constant direct current bias potential of open-circuit voltage with a alternating current (AC) amplitude of 5 mV over the sinusoidal alternating voltage frequency range from 10 mHz to 1 MHz. Cycle life tests were conducted via a CP measurement between -0.05 and 0.35 V at current densities from 1 A g^{-1} to 8 A g^{-1} for 2,000 cycles. The specific capacitance (F g^{-1}) and Coulombic efficiency (%) values determined from the CP curves were calculated according to Eq. (1) & (2):

$$C = \frac{I\Delta T_d}{m\Delta U} \quad (1)$$

$$\eta = \frac{\Delta T_d}{\Delta T_c} \times 100 \quad (2)$$

where C (F g^{-1}), η(%), I(A), $\Delta T_d(s)$, $\Delta T_c(s)$, m(g^{-1}) and ΔU(V) are the specific capacitance, Coulombic efficiency, discharge current, discharge time, charge time, mass of active material in electrode and the potential window used for the measurements respectively.

Results and discussions

Structural and morphological characterizations

XRD technique is used to identify the phase, crystallinity and purity of materials. Fig. 1 shows the XRD pattern of calcinated powder, all the observed peaks are well indexed with the standard peaks indicated by the red lines for cubic $NiCo_2O_4$ material with JCPDS card No. 20-0781. No unidentified peaks are present in the XRD pattern, it indicates the purity of the formed product. The well defined and broad diffraction peaks are also as an indicative of nanocrystalline nature of the sample. XRD pattern of as-prepared precursor before calcination is presented in Fig. S1 (ESI†). All the peaks are well indexed with JCPDS card No. 01-0147 and JCPDS card No. 02-0925 of $Ni(OH)_2$ and $Co(OH)_2$ respectively. So the prepared precursor indicate the formation of hydroxide of Ni and Co and there is no presence of any unidentified peaks.

XPS measurements were carried out in order to understand the oxidation states of different elements on the surface of $NiCo_2O_4$. The XPS spectra are shown in Fig. 2, the full-scan survey spectra of the materials, which indicates the presence of C_{1s} (as reference), O_{1s}, Co_{2p}, and Ni_{2p} as well as the absence of any other impurities is shown in Fig. 2(A). The Co_{2p} spectra is shown in Fig. 2(B) consist of two spin-orbit doublets characteristic of Co^{2+} and Co^{3+}, and two shakeup satellites (indicated as "Satelite."). The fitting peaks at binding energies of Co(II) ions at 781.8 and 797.2 eV are attributed to Co^{2+}, while the other two fitting peaks at 779.4 and 794.8 eV belong to Co^{3+}.[43,44] Similarly, the Ni_{2p} spectra given in Fig. 2(C) are composed of two spin orbit doublets characteristic of Ni^{2+} and Ni^{3+} and two shakeup satellites (indicated as "Satelite".). The fitting peaks at 854.08 and 871.75 eV are indexed to Ni^{2+}, while the other fitting peaks at 855.93 and 873.27 eV are ascribed to Ni^{3+}.[45] The O_{1s} spectra exhibit three main peaks at 532.57, 531.22, and 529.43 eV as shown in Fig. 2(D), associating with hydroxyl species of surface adsorbed water molecule,[44,45] oxygen ions in low coordination at the surface, and the typical of metal–oxygen bonds,[44] respectively. These results show that the surface of the as-synthesized $NiCo_2O_4$ materials has a composition containing Co^{2+}, Co^{3+}, Ni^{2+}, Ni^{3+}, and O^{2-}, which is in good agreement with the results in the literature for $NiCo_2O_4$ spinels.[44-46]

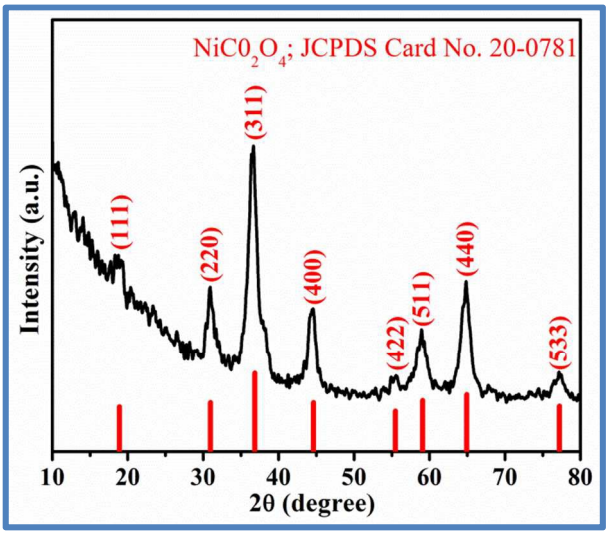

Figure 1. XRD pattern of as-synthesized mesoporous $NiCo_2O_4$ nanosheets

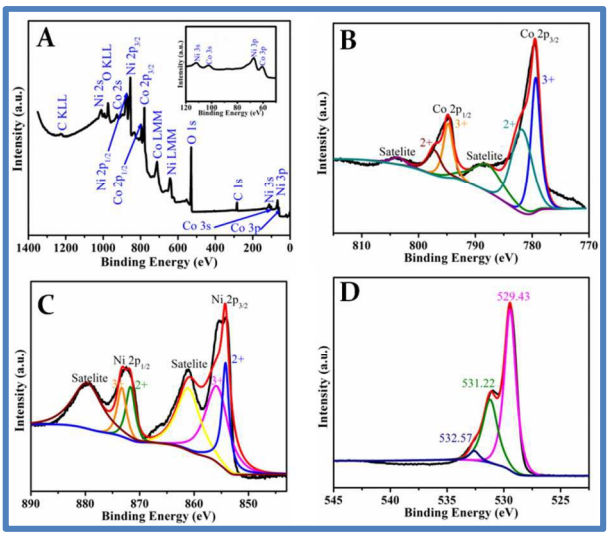

Figure 2. XPS spectra of as-synthesized mesoporous $NiCo_2O_4$ nanosheets (A) full spectrum; (B) Co 2p; (C) Ni 2p; and (D) O 1s.

The specific surface area and the pore structure of as prepared $NiCo_2O_4$ materials were determined using Brunauer-Emmett-Teller (BET) measurements. The porous characteristics of the as prepared $NiCo_2O_4$ were further investigated by typical nitrogen adsorption/desorption isotherms and the results are shown in Fig. 3. As shown in Fig. 3(A) & (B), the curve exhibited the typical Langmuir type IV characteristics with an hysteresis loop which is the inherent property of mesoporous materials. The hysteresis loop in the medium relative high pressure region and its sharp increase of adsorbed N_2 in the high relative pressure region, are the indicative of capillary condensation and multilayer adsorption in the mesopores created. The BET specific surface area, cumulative pore volume, and average pore diameter of the materials is 111.15 $m^2 g^{-1}$, 0.3033 $cm^3 g^{-1}$, and 10.3 nm, respectively. The pore size distribution calculated by Barrett–Joyner–Halenda (BJH) from the adsorption branch also indicates the mesoporous characteristic of the material as shown in Fig. 3(D).[47] It is also evident from Fig. 3(D) that narrow pore size distribution mainly centres in the range of 2.25 -10 nm which is the optimal pore size which provides sufficient active site for Faraday reaction and numerous channels for the diffusion of ions and electrons within the electrode for electrochemical capacitor application.[48-50] So it can be inferred that highly porous structure and large surface area of as synthesized material will greatly enhance the contact area between the electrolyte and electrode, which are beneficial for fast electrochemical reaction. Thus as-prepared mesoporous nanosheets could provide high capacitance and excellent stability as an electrode of electrochemical supercapacitor.

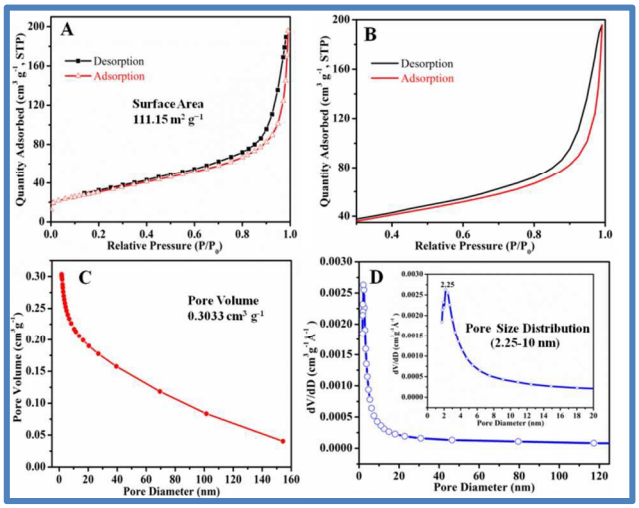

Figure 3. BET plots of mesoporous $NiCo_2O_4$ nanosheets: (A) nitrogen adsorption/desorption isotherms, (B) nitrogen adsorption/desorption isotherms for relative pressure (0.3-1) (B) pore volume distribution, and (C) pore size distribution (Inset: the enlarged view of pore size distribution)

The SEM images of $NiCo_2O_4$ materials are shown in Fig. 4. These as-formed nanosheets with a lateral size of several hundred nanometers are intercrossed with each other, which creates loose porous nanostructures with abundant open space and electroactive surface sites. Transmission electron microscopy (TEM), high resolution transmission electron microscopy (HRTEM) and selected area electron diffraction (SAED) measurements were employed to investigate the microstructure of the mesoporous nanosheets and the crystalline phase of the $NiCo_2O_4$. TEM, HRTEM images with different magnifications and SAED patterns of $NiCo_2O_4$ are displayed in Fig. 5. The inner structure of nanosheets of $NiCo_2O_4$ exhibiting folding silk like morphology with transparent features and it can also be seen that numerous thin nanosheets assembled in all directions with many voids between them as shown in Fig. 5(A) and (B). The lateral size of the nanosheets are much larger than its thickness. The bending, curling and crumpling of nanosheets are observed which is due to their greater lateral size than thickness as shown in Fig. 5(A) and (B). The mesoporous structure of nanosheets is clearly evident as shown in as shown in Fig. 5(C) . The numerous interparticle mesopores are also present in these nanosheets as shown in Fig. 5(C), which results from thermal decomposition of hydroxides and the subsequent recrystallization at a relatively low temperature might facilitate the formation of mesoporous structure. The gaseous species produced during the calcination process also likely to assist in constructing the mesoporous nanosheets. The mesopores mainly originate from the aggregation of small nanoparticles while the large mesopores correspond to void space between the sheets. In order to determine the thickness of nanosheets from the HRTEM, the electron beam was focussed on the vertical cross section at the top of one selected sheet. It can be observed from the HRTEM images that thickness of nanosheets is around 2 nm as shown in Fig. 5(D) . An HRTEM image taken from an individual $NiCo_2O_4$ nanosheet is shown in Fig. 5(E), confirming that the nanosheets are of polycrystalline nature. The clearly resolved lattice fringes were calculated to be about 0.24 nm and 0.28 nm corresponding to the (311) and (220) planes of $NiCo_2O_4$. It is also evident from these images that the dark strips indicate the folded edges or wrinkles of the nanosheets. So the mesoporous and intercrossed feature will facilitate the high transport rates for both electrons and electrolyte ions that simultaneously take part during Faradic reaction. The polycrystalline nature of the synthesized material is also confirmed from the SAED patterns of the nickel cobalt oxides indicating well-defined rings as shown in Fig. 5(F), these rings can be indexed to the (220), (311), (400), (511) and (440) planes of $NiCo_2O_4$ which is in good agreement with the XRD results. It can be envisaged that such $NiCo_2O_4$ nanosheets with fine porous structures and polycrystalline nature may be capable with exciting electrochemical performance.

Electrochemical Evaluation

Cyclic voltammetry (CV) was employed to evaluate the potential of as synthesized $NiCo_2O_4$ acting as an electrode of electrochemical supercapacitor. Fig. 6(A) shows the typical cyclic voltammetry (CV) curves of $NiCo_2O_4$ electrode with various sweep rates ranging from 2 to 30 mV s^{-1} in 2.0 M KOH solution. The shape of the CV curves clearly reveals the pseudocapacitive characteristics. The well defined redox peaks are observed in anodic and cathodic sweeps in all CV curves within the potential range from -0.1 to 0.4 V vs. saturated calomel electrode (SCE) for all sweep rates, which is mainly associated with the Faradaic redox reactions related to M-O/M-O-OH, where M refers to Ni or Co.[30] It is also evident from Fig. 6(A) that even at high scan rate of 30 mV s^{-1}, shape of CVs changes little which is an indicative of the good kinetic reversibility of the $NiCo_2O_4$ modified electrodes. Furthermore Fig. 6(A) also indicates that peak potential shifts only slightly with the increase of scan rate from 2 to 30 mV s^{-1} which is due to low polarization of modified electrode. Therefore, the hybrid electrode is beneficial to fast redox reactions and thus high-power characteristic can be expected. In order to explore the effect of carbon cloth on the capacitance of hybrid nanostructure electrode of $NiCo_2O_4$. CV curve of carbon cloth is shown in Fig. S2 (ESI†) which indicates that the substrate has no contribution towards the pseudocapacitive behaviour of material.

RSC Advances RSCPublishing

PAPER

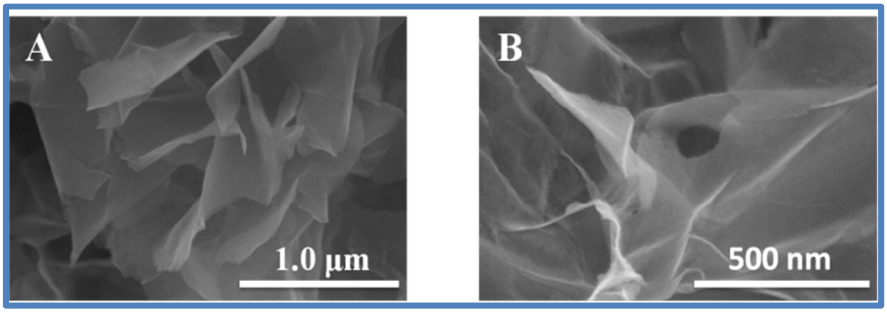

Figure 4. SEM images of mesoporous $NiCo_2O_4$ nanosheets at different magnifications: (A) 1 µm and (B) 500 nm

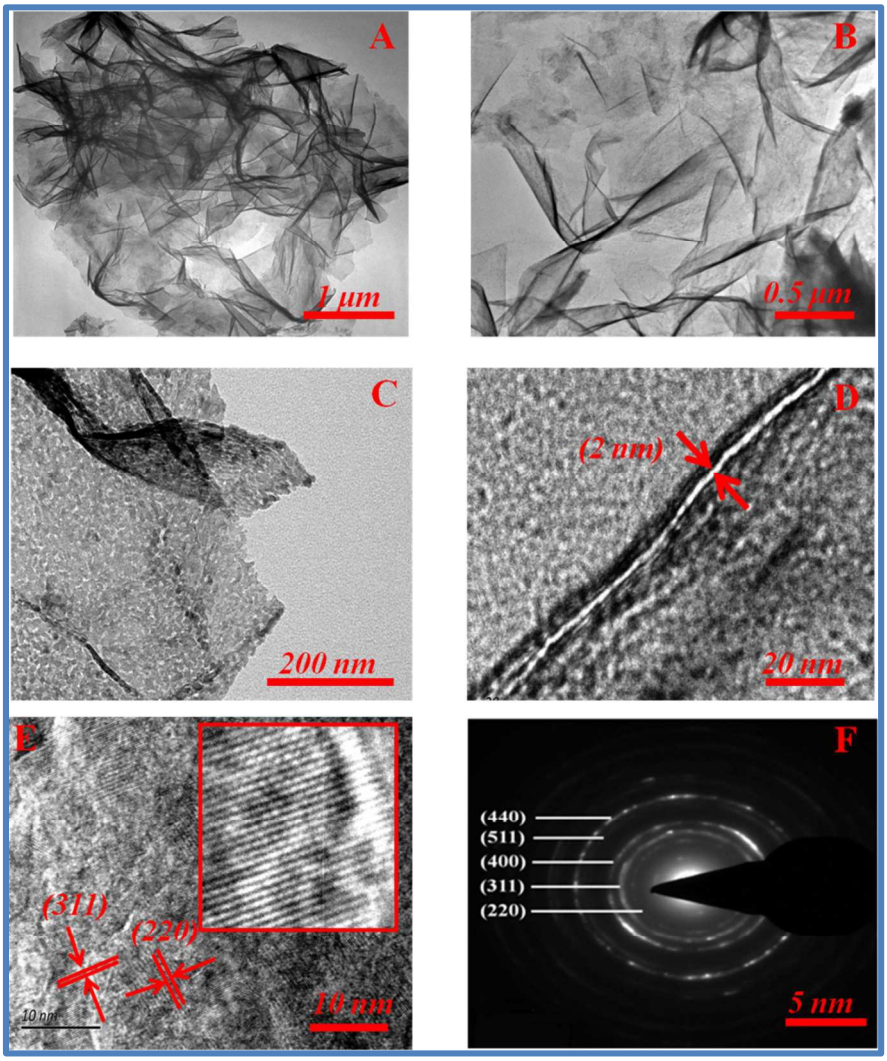

Figure 5. TEM (A, B, C), HRTEM (D,E(Inset: the enlarged view of lattice fringes) and SAED (F) images of mesoporous $NiCo_2O_4$ nanosheets

RSC Advances RSCPublishing

PAPER

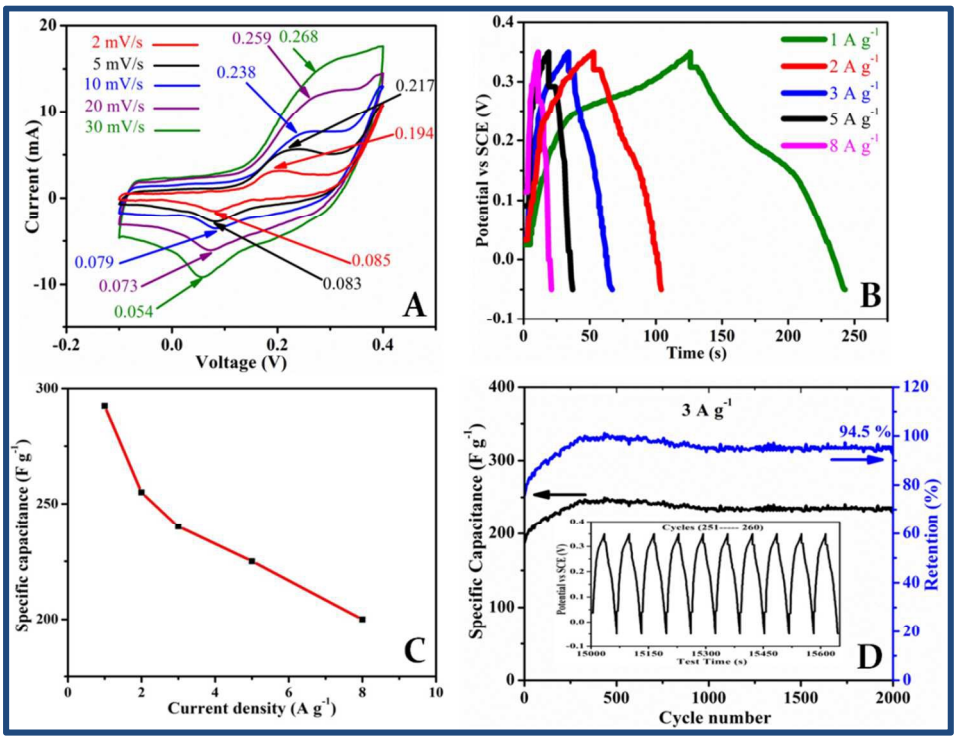

Figure 6. Electrochemical characterization of $NiCo_2O_4$ hybrid nanostructure (A) CV curves at various scan rates ranging from 2 to 30 mV s^{-1}. (B) galvanostatic charge-discharge curves at different current densities (C) specific capacitance as a function of current density, and (D) cycle performance at a current density of 3 A g^{-1}. The inset shows the galvanastic charge - discharge curve at current density of 3 A g^{-1}.

It is also evident from the CV curves that the capacitive property of electrode material is mainly contributed by the Faradaic pseudocapacitance because the integral area of redox peak is far more than the rectangular portion of the curve as shown in Fig. 6 (A). So the contribution of EDL capacitance towards the overall capacitance of electrode is very small. Furthermore, a linear relation between the oxidation peak current and the square root of the scan rate is observed as shown in Fig. S3 (ESI†), which is the confirmation that the redox reaction is a diffusion-controlled process. In order to quantify specific capacitance of as synthesized hybrid structure as an electrode of electrical capacitor, galvanastic charge - discharge measurements were carried out in a 2.0 M KOH electrolyte. The measurements were carried out in the voltage range from -0.05 and 0.35 V vs SCE at various current densities ranging from 1 to 8 A g^{-1} and their corresponding charge-discharge curves are shown in Fig. 6(B). The nonlinearity in the charge-discharge curves further verifies the pseudocapacitive behaviour of $NiCo_2O_4$ orignating from the Faraday reaction. The specific capacitance of hybrid structure electrode of $NiCo_2O_4$ can be calculated on the basis of charge-discharge curves as shown in Fig, 6(B) by using equation (1) and the results are plotted in Fig. 6(C). It is evident from the Fig. 6(C) that with the increase of current density corresponding specific capacitance tends to decrease. The decrease in specific capacitance is attributed to the presence of inner active sites that are unable to sustain the redox transition completely. The CV curve also indicates the incomplete reaction which may be the possible loss of Faradic reaction at higher scan rate 50 and 60 mV s^{-1} as shown in Fig. S4 (ESI†). The specific capacitance of the mesoporous $NiCo_2O_4$ nanosheets electrode is calculated to be about 292.5, 255, 247.5, 225, and 200 F g^{-1} at current densities of 1.0, 2.0, 3.0, 5.0, and 8.0 A g^{-1}, respectively, as shown in Fig. 6(C). It is evident from Fig. 6(C) that 69 % of the capacitance is still retained when the charge discharge rate is increased from 1 to 8 A g^{-1} revealing its excellent rate capability. The cyclic behavior of the $NiCo_2O_4$ electrode at a current density of 3 A g^{-1} is shown in Fig. 6(D). It can be observed from Fig. 6(D), that the specific capacitance increases gradually over the initial cycles accompanying the activation of electrode,[29,51,52] after that the electrode shows the excellent cyclic stability with slight decrease of specific capacitance over 2000 cycles. The penetration of electrolyte ions and the gradual activation of the active materials may be responsible for the increase of the specific capacitance in the first several hundred cycle.[53,54] The retention of specific capacitance is 94.5 % at the end of 2000 cycles at 3 A g^{-1} which is itself remarkable and an indicative of excellent electrochemical stability even

at this high current density. Coulombic efficiency was also calculated by using equation (2) to determine the reversibility of electrode as shown in Fig. S5 (ESI†). Coulombic efficiency increases gradually over the initial cycles accompanying the activation of electrode,[29,51,52] after that the electrode shows the excellent Coulombic efficiency of around 99 % for 2000 cycles which emphasizes its reversible nature as shown in Fig. S5 (ESI†). The galvanastic charge - discharge curves for few cycles at 1 and 3 A g^{-1} are also presented in Fig. S6 (ESI†). The cyclic performance at current density 8 A g^{-1} is also presented in Fig. S7 (ESI†). The excellent capacitance retention of 90 % is observed at the end of 2000 cycles at 8 A g^{-1} as shown in Fig. S7 (ESI†). The cycling stability of flexible supercapacitor was investigated by performing its cyclic test under bending state. In the bend state, the cyclic performance indicates excellent capacitance retention of 89 % after 2000 cycles at current density of 3 A g^{-1} as shown in Fig. S8(ESI†). The cyclic test also indicates almost the same performance in the bend state as shown in Fig. S8(ESI†) in comparison with normal state as shown in Fig. 6 (D). So the electrochemical performance of supercapacitor do not significantly change in the bend state confirming its application as a flexible supercapacitor. SEM measurements of fresh and used electrodes were carried out to determine the structural changes as a result of long term cyclic test as shown in Fig. S9(A,B,C) & (D,E,F)(ESI†) respectively. The basic morphology of the $NiCo_2O_4$ is overall well preserved as shown in Fig. S9(D,E,F). These results demonstrate that the carbon cloth supported $NiCo_2O_4$ electrodes possess the essential characteristics for high-performance supercapapacitor, and meet the requirements of long-term stability. In comparison with the other reported $NiCo_2O_4$ nanosheets and nanowires on carbon cloth,[36] the capacitance value obtained for nanosheets in our work at 1 A g^{-1} is 292.5 F g^{-1}, which is much higher than the reported capacitance values 123 and 245 F g^{-1} for nanosheets and nanowires respectively.[36] In case of our work supercapacitor exhibited cyclic operation for 2000 cycles which is much higher than the reported work for only 1000 cycles.[36] In our case specific surface area and pore volume are 111.15 m^2 g^{-1} and 0.3033 cm^3 g^{-1} respectively, which are much higher than that of reported for nanosheets (28.22 m^2 g^{-1}, 0.11 cm^3 g^{-1}) and nanowires (79.34 m^2 g^{-1}, 0.26 cm^3 g^{-1}).[36] The more narrow and ordered distribution of pores at ~ 2.25 nm in our case than that of reported nanosheets (~ 3.04, 4.97, 12.46, and 26.44 nm) and nanowires (~ 4.86 nm).[36] So high capacitance value is orignating from the mesoporous, high specific surface area and large pore volume of the synthesized material which provides numerous electroactive sites for redox reaction. Furthermore as evidenced from the SEM and TEM measurements that open space between these nanosheets and mesopores existing in the nanosheets can serve as a reservoir for ions and also greatly enhance the diffusion kinetics within the electrode. Actually the mesoporous structure, high specific surface area and narrow pore distribution of nanosheets are fully responsible for the excellent contact between the electrolyte and electroactive nanosheets even at higher rates. These results evidently suggest the great promise of this mesoporous $NiCo_2O_4$ nanosheets electrode for high-performance ECs characterized by both long cycle life and excellent rate capability. To further evaluate the electrochemical behavior of electrode, electrochemical impedance spectroscopy (EIS) was performed. EIS plots of the $NiCo_2O_4$ electrode in fresh and after 2,000 CP cycles is presented in Fig. 7(A) & (B). It is evident from this graph that the Nyquist plots consist of a semicircle in the high frequency region and a declined line deviating 90° in the low-frequency region, whereas the Nyquist plots after 2,000 cycles exhibits a larger semicircle and a more deviated angle associating with the larger electrochemical polarization. The experimental data can be fitted by Randles equivalent circuit as shown in the inset of Fig. 7(A) &(B), where R_s is the internal resistance, which contains the inherent resistance of the electro active material, bulk resistance of electrolyte, and contact resistance at the interface between electrolyte and electrode,[55] R_{ct} is the charge transfer resistance, W is the Warburg impedence, CPE_1 is the electric double layer capacitance and CPE_2 is the pseudocapacitance. The internal resistance R_s and charge transfer resistance R_{ct} can be determined from the intercepts of high frequency semicircle on the real axis which corresponds to R_s and (R_s + R_{ct}) respectively.[56,57] The simulated impedence values of fresh and used electrodes are presented in Table 1 & 2(ESI†) respectively. The simulated internal resistance R_s and charge transfer resistance R_{ct} for fresh and used electrodes are 0.5876 Ω , 1.957 Ω and 0.9045 Ω, 2.061 Ω respectively. These relatively smaller R_s and R_{ct} values are also an indication of good electronic conductivity of active electrode materials which are responsible for the high performance and excellent rate capability of our synthesized supercapacitor electrode. These relatively smaller R_s and R_{ct} values are due to the fact that mesoporous nanosheets facilitate the efficient access of electrolyte ions to active materials by shortening the ion diffusion path, which is an important factor and play vital role in obtaining the high performance of supercapacitor electrode.

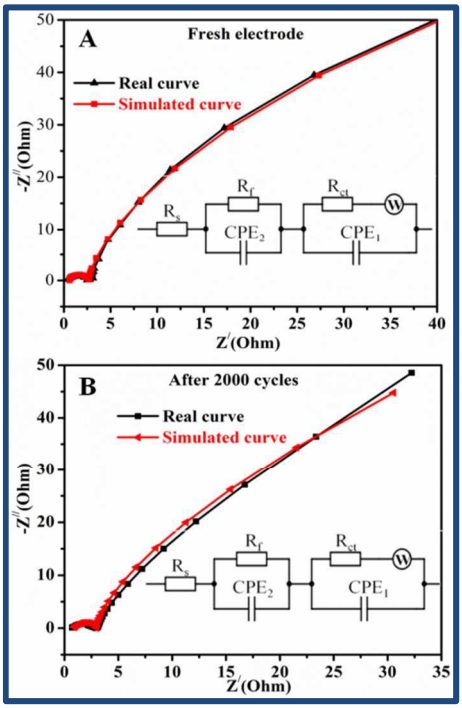

Figure 7. EIS plots of the as-synthesized $NiCo_2O_4$-modified electrode in 2.0 M KOH solution (A) fresh and (B) after the cycle test (Inset: Randles equivalent circuit)

Conclusions

Mesoporous $NiCo_2O_4$ nanosheets are synthesized via a facile and cost-effective microwave assisted method followed by a simple thermal treatment at 300°C. The as- prepared material is composed of mesoporous nanosheets with the thickness of around 2 nanometer. These mesoporous nanosheets have high specific surface area, large pore volume and narrow pore size distribution. The mesoporous $NiCo_2O_4$ nanosheets on carbon cloth exhibit excellent pseudocapacitive behavior with the features of specific capacitance (292.5 F g^{-1} at 1 A g^{-1}) and excellent cycling stability even at the high charge/discharge rate. The capacitance retention of 94.5 and 90 % are observed even after continuous 2000 cycles of charge/discharge at 3 and 8 A g^{-1} respectively. The excellent capacitance retention of 89 % is also observed in the bend state at 3 A g^{-1}. The basic morphology of the $NiCo_2O_4$ is overall well preserved after the cycle test. The excellent specific capacitance and capacity retention of as synthesized material are mainly because of the existence of interparticle mesopores, high surface area, low internal resistance (R_s) and large pore volume of nanosheets. Our results indicate that the mesoporous $NiCo_2O_4$ nanosheets on carbon cloth are highly desirable in the application of advanced flexible electrode for supercapacitors.

Acknowledgments

This work was supported by National Natural Science Foundation of China (21371023, 50972017), the Research Fund for the Doctoral Program of Higher Education of China (20101101110026).

References

1 S. Cheng, L. Yang, Y. Liu, W. Lin, L. Huang, D. Chen, C.P. Wong and M. Liu, *J. Mat. Chem. A*, 2013, 1, 7709-7716.
2 S. Wang and R.A.W. Dryfe, *J. Mat. Chem. A*, 2013, 1, 5279-5283.
3 Q. Wang, X. Wang, B. Liu, G. Yu, X. Hou, D. Chen and G. Shen, *J. Mat. Chem. A*, 2013, 1, 2468-2473.
4 W. Wei, X. Cui, W. Chen and D.G. Ivey, *Chem. Soc. Rev*., 2011, 40, 1697-1721.
5 G. Wang, L. Zhang and J. Zhang, *Chem. Soc. Rev*., 2012, 41, 797-828.
6 P. Simon and Y. Gogotsi, *Nat. Mater.,* 2008, 7, 845-854.
7 J. R. Miller and P. Simon, *Science,* 2008, 321, 651-652.
8 C. Yang, L. Dong, Z. Chen and H. Lu, *J. Phy. Chem. C*, 2014, 118, 18884–18891.
9 N. Garg, M. Basu and A. K. Ganguli, *J. Phy. Chem. C*, 2014, 118, 17332–17341.
10 M. Grdeń, M. Alsabet and G. Jerkiewicz, *ACS Appl. Mat. Interfaces*, 2012, 4, 3012-3021.
11 W. Xing, S. Qiao, X. Wu, X. Gao, J. Zhou, S. Zhuo, S.B. Hartono and D. Hulicova-Jurcakova, *Journal of Power Sources*, 2011, 196, 4123-4127.
12 Q. Cheng, J. Tang, J. Ma, H. Zhang, N. Shinya and L.-C. Qin, *J. Phy. Chem. C*, 2011, 115, 23584-23590.
13 B. E. Conway, Electrochemical Supercapacitors: Scientific Fundamentals and Technological Applications , Kluwer Academic/Plenum Publishers New York 1999.
14 C. Z. Yuan, B. Gao, L. F. Shen, S. D. Yang, L. Hao, X.J. Lu, F. Zhang, L.J. Zhang and X.G. Zhang, *Nanoscale*, 2011, 3, 529-545.
15 J. Xiao and S. Yang, *RSC Adv*., 2011, 1, 588-595.
16 T. Brezesinski, J. Wang, S. H. Tolbert and B. Dunn, *Nat. Mater*., 2010, 9, 146-151.
17 W. Sugimoto, H. Iwata, Y. Yasunaga, Y. Murakami and Y. Takasu, *Angew. Chem. Int. Edit*., 42 (2003) 4092-4096.
18 C. Yuan, L. Chen, B. Gao, L. Su and X. Zhang, *J. Mat. Chem*., 2009, 19, 246-252.
19 J.-K. Chang, C.-T. Lin and W.-T. Tsai, *Electrochem. Commun*., 2004, 6, 666-671.
20 V. Subramanian, H. Zhu, R. Vajtai, P. M. Ajayan and B. Wei, *J. Phy. Chem. B,* 2005, 109, 20207-20214.
21 K. C. Liu and M. A. Anderson, *J. Electrochem. Soc*., 1996, 143, 124-130.
22 C. Yuan, B. Gao, L. Su and X. Zhang, *Solid State Ionics,* 2008, 178, 1859-1866.
23 C. Zheng, C.Cao, Z. Ali and J.Hou, *J. Mat. Chem. A*, 2014, 2, 16467-16473.
24 Y. Gao, S. Chen, D. Cao, G. Wang and J. Yin, *J. Power Sources*, 2010, 195, 1757-1760.
25 S. Xiong, C. Yuan, X. Zhang, B. Xi and Y. Qian, *Chem-Eur. J.,* 2009, 15, 5320-5326.
26 M.-S. Wu and K.-C. Huang, *Chem. Commun*., 47 (2011), 47, 12122-12124.
27 Y. Zhu, C. Cao, S. Tao, W. Chu, Z. Wu and Y. Li, *Sci. Rep*., 2014, 4.
28 Y. Fu, J. Song, Y. Zhu and C. Cao, *J. Power Sources*, 2014, 262, 344-348.
29 T.-Y. Wei, C.-H. Chen, H.-C. Chien, S.-Y. Lu and C.-C. Hu, *Adv. Mat*., 2010, 22, 347-351.
30 H. Wang, Q. Gao and L. Jiang, *Small,* 2011, 7, 2454-2459.
31 H. Jiang, J. Ma and C. Li, *Chem. Commun*., 2012, 48, 4465-4467.
32 R. Alcántara, M. Jaraba, P. Lavela and J.L. Tirado, *Chem. Mater*., 2002, 14, 2847-2848.
33 N. Padmanathan and S. Selladurai, *RSC Adv*., 2014, 4, 8341-8349.
34 D. Zhang, H. Yan, Y. Lu, K. Qiu, C. Wang, C. Tang, Y. Zhang, C. Cheng and Y. Luo, *Nanoscale Res. Lett*., 2014, 9, 139.
35 F. Luan, G. Wang, Y. Ling, X. Lu, H. Wang, Y. Tong, X.-X. Liu and Y. Li, *Nanoscale*, 2013, 5, 7984-7990.
36 H. Wang, X. Wang, *ACS Appl. Mat. Interfaces,* 2013, 5, 6255-6260.
37 S. K. Meher and G.R. Rao, *J. Phy. Chem. C,* 2011, 115, 25543-25556.
38 S. Faraji and F.N. Ani, *J. Power Sources,* 2014, 263, 338-360.
39 Y. Ding, L. Xu, C. Chen, X. Shen and S.L. Suib, *J. Phy. Chem. C,* 2008, 112, 8177-8183.
40 L. Xu, Y.-S. Ding, C.-H. Chen, L. Zhao, C. Rimkus, R. Joesten and S.L. Suib, *Chem. Mater*., 2007, 20, 308-316.
41 I. Bilecka and M. Niederberger, *Nanoscale*, 2010, 2, 1358-1374.
42 M. Baghbanzadeh, S.D. Škapin, Z.C. Orel and C.O. Kappe, *Chem-Eur. J*., 2012, 18, 5724-5731.
43 Y.E. Roginskaya, O.V. Morozova, E.N. Lubnin, Y.E. Ulitina, G.V. Lopukhova and S. Trasatti, *Langmuir,* 1997, 13, 4621-4627.
44 J. F. Marco, J. R. Gancedo, M. Gracia, J. L. Gautier, E. Rıos and F.J. Berry, *J. Solid State Chem*., 2000, 153, 74-81.
45 J. G. Kim, D.L. Pugmire, D. Battaglia and M. A. Langell, *Appl. Surf. Sci*., 165 (2000), 165, 70- 84.
46 A. Thissen, D. Ensling, F.J. Fernández Madrigal, W. Jaegermann, R. Alcántara, P. Lavela and J.L. Tirado, *Chem. Mater*., 2005, 17, 5202-5208.

47 J. Li, S. Xiong, Y. Liu, Z. Ju and Y. Qian, *ACS Appl. Mat. Interfaces,* 2013, 5, 981-988.
48 G. Q. Zhang, H.B. Wu, H.E. Hoster, M.B. Chan-Park and X.W. Lou, *Energ. Environ. Sci*., 2012, 5, 9453-9456.
49 H. Zhou, D. Li, M. Hibino and I. Honma, *Angew. Chem. Int. Edit.,* 2005, 44, 797-802.
50 Y. Chen, B. Qu, L. Hu, Z. Xu, Q. Li and T. Wang, Nanoscale, 2013, 5 9812-9820.
51 C. Yuan, J. Li, L. Hou, X. Zhang, L. Shen and X.W. Lou, *Adv. Funct. Mater*. 2012, 22, 4592-4597.
52 Y. Lei, J. Li, Y. Wang, L. Gu, Y. Chang, H. Yuan and D. Xiao, *ACS Appl. Mat. Interfaces* 2014, 6, 1773-1780.
53 Y.-T. Wu and C.-C. Hu, *J. Electrochem. Soc*. 2004, 151, A2060-A2066.
54 C.-C. Hu, K.-H. Chang and T.-Y. Hsu, *J. Electrochem. Soc*., 2008, 155, F196-F200.
55 C. Yuan, X. Zhang, Q. Wu and B. Gao, *Solid State Ionics,* 2006, 177, 1237-1242.
56 K. P. Wang and H. S. Teng, *J. Electrochem. Soc.,* 2007, 154, A993-A998
57 C. W. Huang and H. S. Teng, *J. Electrochem. Soc.,* 2008, 155, A739-A744